

# Self-assembled Diphenylalanine Peptide Fibrils with Ultra-High Aspect Ratio: A Platform for Sensitive Electrochemical H<sub>2</sub>O<sub>2</sub> Sensor

Yuehong Pang, Qiufang Zhang, Xiulan Sun, Jian Ji, Fuwei Pi, Xiaofang Shen\*

State Key Laboratory of Food Science and Technology, School of Food Science and Technology, Jiangnan University, Wuxi, 214122, China

\*E-mail: [xfshen@jiangnan.edu.cn](mailto:xfshen@jiangnan.edu.cn)

Received: 3 May 2018 / Accepted: 6 June 2018 / Published: 5 August 2018

---

Inspired from the pathogenic process of diphenylalanine (FF) self-assembly, a key structural motif in forming Alzheimer's  $\beta$ -amyloid peptide fibrils, a facile way for preparation of FF aromatic dipeptide fibrils and fabrication of an electrochemical biosensor were developed. Long persistence length FF fibrils with ultra-high aspect ratio over 1000 were obtained using cationic surfactant assisted evaporation induced self-assembly. The Cotton effects indicate a signature of dominant  $\beta$ -sheet arrangement and the thickness of the  $\beta$ -sheet monolayer is estimated to be 2.38 nm. The obvious blue-shift of intrinsic fluorescence indicates an extended H-aggregate between the phenyl rings in a parallel mode. The FF fibrils based electrochemical biosensor, taking horseradish peroxidase as a model enzyme, displayed an excellent electrocatalytic activity to the reduction of H<sub>2</sub>O<sub>2</sub>. The peak current was a linear function of concentrations ranging from  $7.5 \times 10^{-7}$  to  $1.4 \times 10^{-5}$  M, with a detection limit of  $2.5 \times 10^{-7}$  M. The apparent Michaelis-Menten constant was 7.2  $\mu$ M. These results indicate that the FF fibrils with ultra-high aspect ratio providing a new and promising platform for construction of electrochemical biosensors.

---

**Keywords:** Diphenylalanine; Aromatic dipeptide; Self-assembly; Nanofibrils; Electrochemical Biosensor

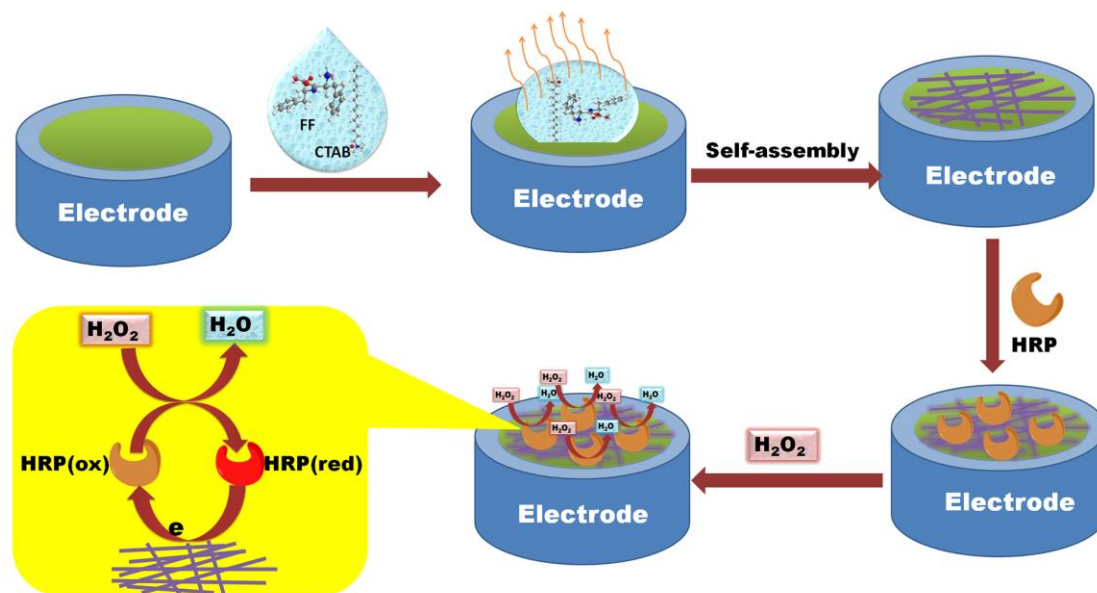
## 1. INTRODUCTION

The efficacy of the electrochemical biosensing device can be improved by careful choice of novel functional micro- and nanomaterials [1-3]. These materials fabricated from biological building blocks have excellent biocompatibility. Many biomolecules, such as peptide, can self-assemble into highly ordered architectures with aimed functionality [2-6]. The peptide building blocks can interact

with each other to form supramolecular structures via non-covalent interactions, including ionic, hydrophobic, hydrogen bonding and  $\pi$ - $\pi$  stacking [7]. A known example is the diphenylalanine (FF) aromatic dipeptide, a key structural motif in forming amyloid peptide fibrils by Alzheimer's  $\beta$ -amyloid peptide [8]. Inspired from the pathogenic process, researchers find that FF can spontaneously assemble into nanotubes and spherical vesicles, as well as form new ordered nanoarchitectures. These peptide-based micro- and nanomaterials are believed to be important for next generation of biosensors not only because of their high biocompatibility but also their remarkable thermal and chemical stability [9]. It is reported that remarkable metallic-like point stiffness of FF dipeptide nanospheres is up to  $885 \text{ N m}^{-1}$  and Young's modulus up to  $275 \text{ GPa}$  [10]. These nanostructures are reported to date as the stiffest organic materials, even than macroscopic aramids. Interestingly, FF nanowire structures are in high stability up to  $200^\circ\text{C}$  and no changes in pH 1 to 14 aqueous solutions or in polar to non-polar solvents [11].

Extensive coarse-grained molecular dynamics simulations of the FF assembly pathway find that the dipeptides not only spontaneously assemble into spherical vesicles and nanotubes, but also can form ordered nanoarchitectures [12]. Energetic analysis suggests that the delicate balance between peptide-peptide and peptide-water interactions results in the formation of different nanostructures. The interactions between the hydrophobic side chains play an important role in the formation of the assemblies. Simulation of crystalline structural fragments also shows that the strongest interactions occur between side chains rather than between charged terminals. Furthermore, the amphiphilic nature of FF is the most important to understand its self-assembly, and that the early precursors to nanotube structures are possibly involved in substantial hydrophobic clustering [13]. Therefore, to control the morphologies of the resultants in FF self-assembled micro- and nanostructures, the surrounding microenvironment for the hydrophobic aromatic sides in the precursor solutions should be created.

Soft template synthesis using various surfactant aggregates may be a more general method. The non-covalent interactions induced self-assembly of surfactants provides a powerful tool for building well-defined nanostructures [14]. The quaternary ammonium salt cationic surfactant is the most commonly used in the shape-controlled synthesis due to their hydrophobic chains linked to charged hydrophilic heads [15]. In this paper, we demonstrate a facile way for evaporation induced self-assembly of FF dipeptide and fabrication of an electrochemical biosensor (as schematically illustrated in Fig. 1). A typical cationic surfactant of CTAB assisted preparation was performed under a mild condition and the resultants are fibrils with ultra-high aspect ratio. The FF fibrils based biosensor, taking horseradish peroxidase (HRP) as a model enzyme, was obtained and high sensitivity was displayed. The biosensor constructed on the bio-inspired peptide fibrils also demonstrated good reproducibility, selectivity, long-term stability and low detection limit for  $\text{H}_2\text{O}_2$  detection.



**Scheme 1.** Schematic illustration of the preparation of FF ultra-long peptide fibrils using CTAB assisted evaporation induced self-assembly and the fabrication of hydrogen peroxide electrochemical biosensor.

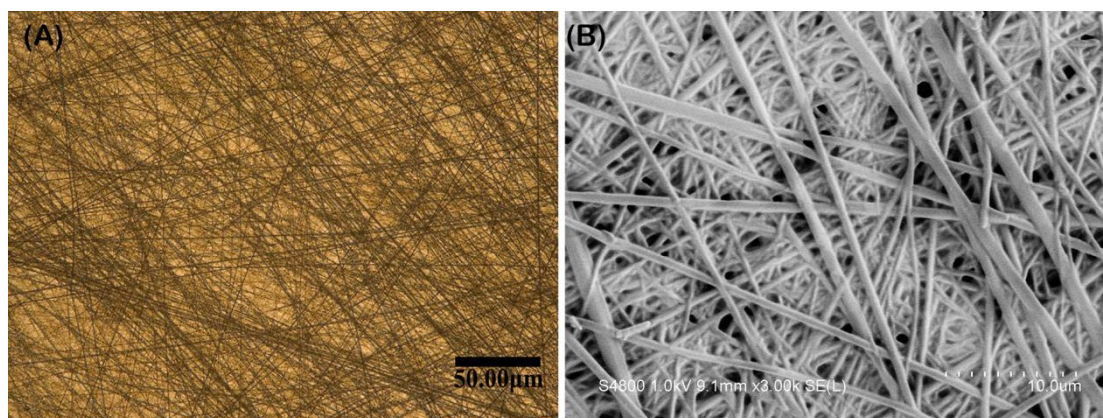


**Figure 1.** (a) The optical microscope and (b) SEM images of the FF fibrils.

## 2. EXPERIMENTAL

### 2.1 Materials

Diphenylalanine (FF) was purchased from Bachem. 1,1,1,3,3,3-hexafluoro-2-propanol (HFP) was obtained from Aladdin (Shanghai, China). Hexadecyl trimethyl ammonium bromide (CTAB) and 30%  $\text{H}_2\text{O}_2$  aqueous solution, HRP (250 U  $\text{mg}^{-1}$ ) were purchased from National Medicine Group Chemical Reagent Co., Ltd. Mixing the stock standard solutions of  $\text{Na}_2\text{HPO}_4$  and  $\text{NaH}_2\text{PO}_4$ , the 0.1 M phosphate buffer solutions (PBS) with different pH values were prepared. All chemicals and solvents were analytical grade and all solutions were prepared with twice-distilled deionized water.

## 2.2 Apparatus

Powder X-ray diffraction (XRD) was conducted on a D8 X-ray diffractometer (Bruker AXS, Japan). Scanning electron microscopy (SEM) image was taken by an S-4800 scanning electron microscope (Hitachi, Japan). Optical microscope images were taken by an AM413T5 digital optical microscope (Suzhou Oka optical Ltd., China). Fourier transform infrared spectra (FTIR) analysis was carried out by using an IS10 Fourier infrared spectrometer (Nicolet, America). circular dichroism (CD) analysis was carried out by using a MOS-450 circular dichroism spectrometer (Bio-Logic, France). Fluorescence analysis was carried out using an F-7000 Fluorescence spectrophotometer (Hitachi, Japan). Cyclic voltammetric (CV) and amperometric experiments were carried out with a CHI660c electrochemical workstation (Chenhua, China). A conventional three electrode cell with FF fibrils modified glassy carbon electrode (GCE, diameter=3 mm) as the working electrode, a platinum wire as the auxiliary electrode and a saturated calomel electrode (SCE) as the reference electrode.

## 2.3 Preparation of FF fibrils

In a typical process, 1.00 mg FF was dissolved in 20  $\mu\text{L}$  HFP and then volume-equally 4 mM CTAB was added into the solution. 10  $\mu\text{L}$  of mixture was transferred to a clean glass slide or GCE using a fresh pipet tip and then self-assembled for 12 h at 30°C. Allowed the solvent evaporation under a controlled relative humidity at 0.75. It was further incubated inside a humid chamber overnight for the purpose of the full development of peptide nanostructures. With the evaporation of the solvent, FF ultra-long fibrils were obtained.

## 2.4. Fabrication of FF fibrils-based electrochemical biosensor

GCE was polished carefully to a mirror-like by 0.3 and 0.05  $\mu\text{m}$  alumina slurry and then ultrasonically cleaned in ethanol and ultrapure water. At last, the electrode was dried with nitrogen gas. The FF fibrils were self-assembled on the substrate of GCE by the above mentioned method. The HRP stock solution was prepared by dissolving 2 mg HRP in 100  $\mu\text{L}$  PBS buffer (pH 7.0). Then, 20  $\mu\text{L}$  HRP solution was dropped on the surface of FF fibrils modified GCE and allowed to dry under ambient condition.

# 3. RESULTS AND DISCUSSION

## 3.1 Self-assembly of the FF ultra-long fibrils

Aromatic interactions between the molecules of FF were considered to be critical for the formation of  $\beta$ -amyloid fibrils, which induced the Alzheimer's disease<sup>[8]</sup>. FF tends to form a tubular structure in aqueous solution due to aromatic stacking of FF molecules in a hierarchical array surrounding water clusters tightly [16]. Therefore, we choose a typical cationic surfactant of CTAB,

whose hydrophobic chains are buried from water and charged sides are situated on the water-exposed surface, to prevent the formation of water channels assembled by FF. With the assistance of CTAB, we prepared ultra-long FF fibrils on solid substrates using solvent-vapor growth method.

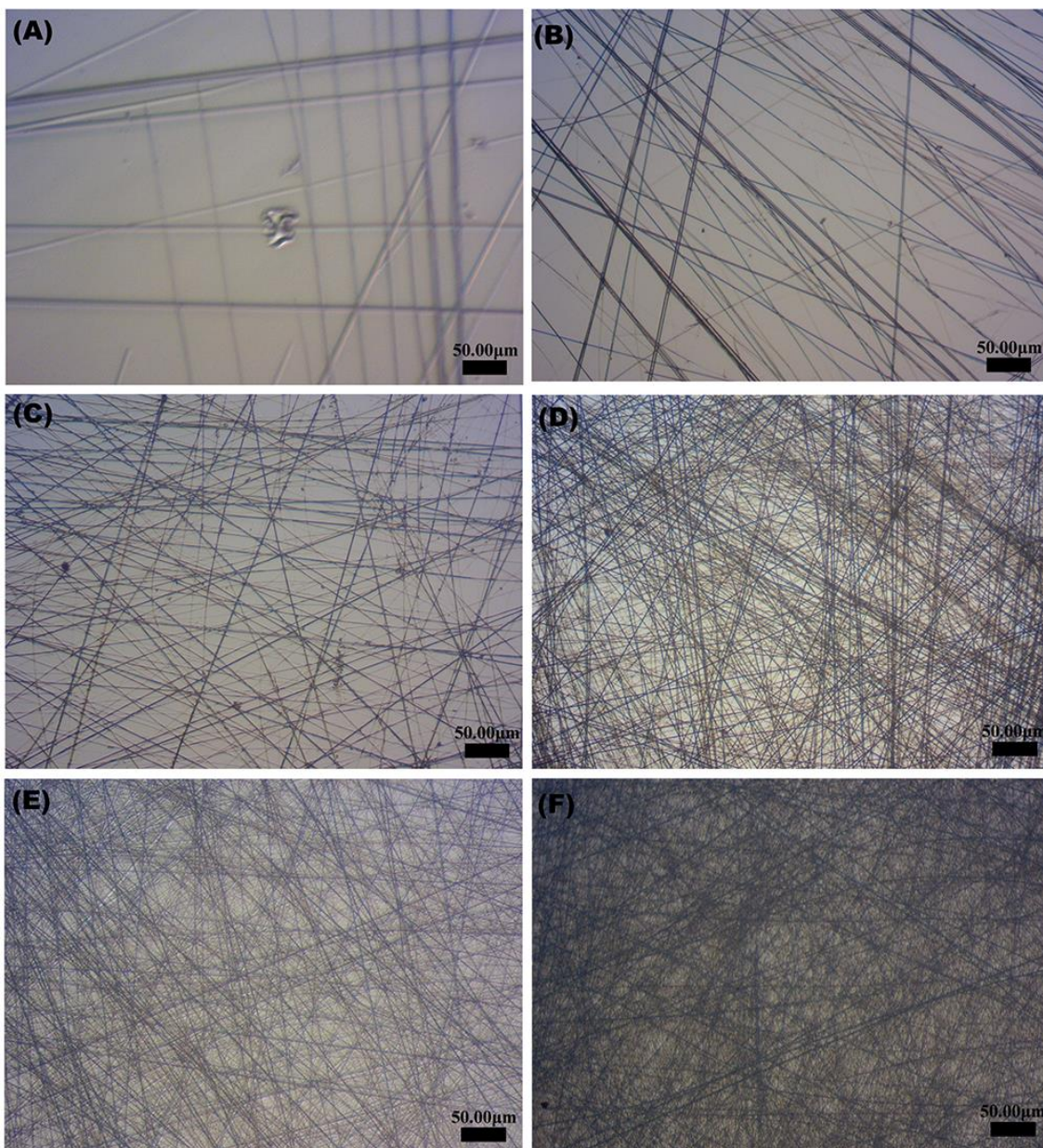


**Figure 2.** Optical microscope images of FF fibrils preparing with different molar ratios of CTAB to FF, (a) 1:40, (b) 1:13, (c) 1:5, (d) 1:3.2, (e) 1:2.5, (f) 1:1.7.

The topographical information of the resultants was obtained by optical microscope and SEM (Fig.2). Diameters of the FF fibrils range from about 100 nm to 1  $\mu\text{m}$ . It is reported that one dimensional nanostructures with high-aspect-ratio have large surface-to-volume ratios, which are suitable for biomedical applications [17-18]. Note that the as-prepared FF fibrils have a long persistence length over millimeters. Thus, these fibrils have a very high aspect ratio of more than 1000. Generally, high aspect ratio 1D nanostructures were obtained by hydrothermal method [19], hard

template fabrication [20] or metal-assisted chemical etching [21] and so on. The soft templates can be used to control the shape and size to prepare 1D nanostructures with high aspect ratios [22]. Here, the aromatic amino acid of FF are easily embedded inside the cationic surfactant micelles, wherein the  $-NH_2$  and  $-COOH$  groups interact with hydrophilic headgroups of the surfactant, and the phenyl group associates with the hydrophobic site. These interactions bring about the formation of the FF fibrils with ultra-high aspect ratio.

We propose that evaporation of the solvent results in a supersaturation of FF, which facilitates to reach the critical micelle concentration of CTAB. Therefore, we fixed the concentration of the FF and changed the molar ratios of CTAB and FF to observe the morphology changes of the resultants (Fig 2). At low concentration of CTAB (CTAB to FF are 1:40 and 1:13, shown in Fig 2a and 2b), several fibrils are formed with diameters of about 7  $\mu m$  and 5  $\mu m$ , respectively. Further increase the amount of CTAB made the diameters of the fibrils reduce dramatically. The resultant fibrils in Fig 2d, Fig 2e and 2f showed the uniform and smooth morphologies. The diameter of the formative 1D fibrils were significantly decreased with the increase of CTAB.

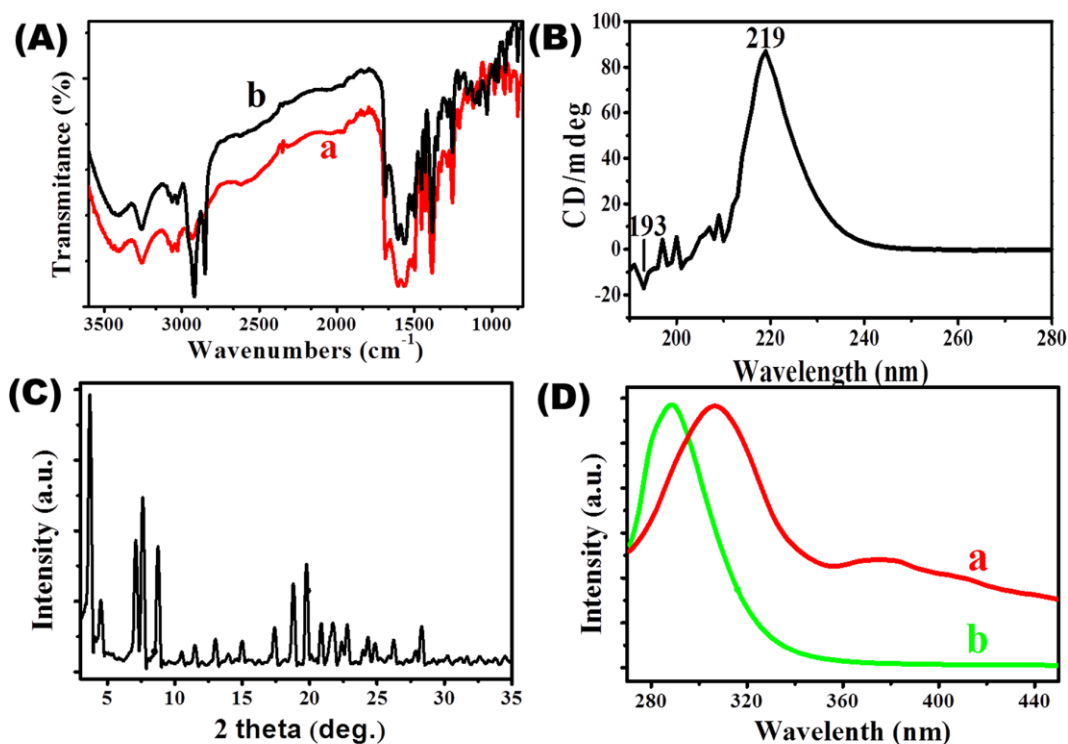


**Figure 3.** (A) The FTIR spectra of (a) FF powder and (b) FF fibrils; (B) CD spectrum of FF fibrils; (C) XRD patterns of FF fibrils; (D) Normalized FL spectrum ( $\lambda_{excitation} = 265$  nm) of (a) FF in DMF and (b) FF fibrils.

FTIR of FF powder and the as-prepared FF fibrils were shown in Fig.3. Strong amide I absorption bands in the vicinity of  $1687\text{ cm}^{-1}$  indicates the predominant hydrogen-bonded  $\beta$ -sheet secondary structures with an anti-parallel configuration [23-27]. Compared with powder, FTIR spectrum of fibrils shows two strong absorption bands in  $3000\text{--}2840$  and  $1487\text{ cm}^{-1}$ , which are caused

by the symmetrical and anti-symmetrical stretching vibration of  $\text{CH}_3^-(\text{N}^+)$ , and the anti-symmetrical angle of vibration of  $\text{CH}_3^-(\text{N}^+)$ , assigned to the CTAB [28]. In addition, position, shape and the relative intensity of FF fibrils are similar to FF powder, indicating no chemical bond formed during the process of self-assembly. Non-covalent interactions among peptides, such as ionic, hydrophobic, hydrogen bonding and  $\pi$ - $\pi$  stacking, are helpful to form these micro- and nanostructures. Therefore, circular dichroism (CD) spectra (Fig. 2B), X-ray diffraction (XRD) (Fig. 2C) and fluorescence (Fig. 2D) were used to characterize the FF fibrils for further understanding the mechanism. The Cotton effects for the FF fibrils at characteristic peaks of 193 and 219 nm can be interpreted as signatures of dominant  $\beta$ -sheet arrangements [29-32]. The band at 193 nm corresponds to the  $\pi \rightarrow \pi^*$  transition, and the broad positive band centered on 219 nm is indicated to an  $n \rightarrow \pi^*$  transition. Four correlative diffraction peaks of  $3.71^\circ$ ,  $7.59^\circ$ ,  $19.75^\circ$  and  $28.34^\circ$  in the XRD patterns are observed, which correspond to  $d$  spacings of 23.79, 11.71, 4.48 and 3.14 Å, respectively. The thickness of the  $\beta$ -sheet monolayer in the fibrils is estimated to be about 2.38 nm. Each FF molecule contains two aromatic amino acid residues of phenylalanine, which may contribute to its intrinsic fluorescence. A striking feature of the structure is using phenylalanine side chains to stabilize the inter-sheet packing by means of  $\pi$ - $\pi$  stacking. The importance of aromatic rings  $\pi$ - $\pi$  stacking has been demonstrated in FF nanotubes<sup>[8]</sup>, which is attractive in general FF self-assembly. The fluorescence of FF powder dissolved in DMF was observed at an emission maximum ( $\lambda_{\text{max}}$ ) around 306 nm, which is an intrinsic property of the monomeric unit itself due to the presence of aromatic side chain residues. After self-assembling into fibrils, the emission peak shifted to 288 nm. The obvious blue-shift indicates an extended H-aggregate between the phenyl rings in a parallel mode. The aggregates are similar to the organization of  $\pi$ - $\pi$  stacking in self-assembled amyloid fibrils [33-35].

FF nanoforest-based biosensor for phenol detection was more sensitive than those modified with carbon nanotubes [36]. The FF-based biosensor provides a novel platform with high biocompatibility. Herein, the FF fibrils could be self-assembled on the working electrode for electrochemical biosensors. Fig. 4A shows the relative CV responses for (a) bare GCE, (b) FF fibrils/GCE, (c) FF powder/GCE in 50 mM  $[\text{Fe}(\text{CN})_6]^{3-/4-}$  solution containing 0.1 M KCl. After modified with FF powder, both the oxidation and reduction currents of the electrode were obviously decreased and the peak-to-peak separations were enlarged ( $\Delta E_p=157$  mV). While self-assembled with fibrils, the redox peak currents and the reversibility ( $\Delta E_p=78$  mV) of the electrode were equivalent to the bare GCE. The result demonstrates that FF fibrils have a good electrochemical activity. CV was also employed to evaluate the stability of FF fibrils film (Fig. 4B). Both the oxidation and reduction peak currents of FF fibrils modified electrode kept over 99% of its initial response after 100 circles scanning (Fig. 4B).

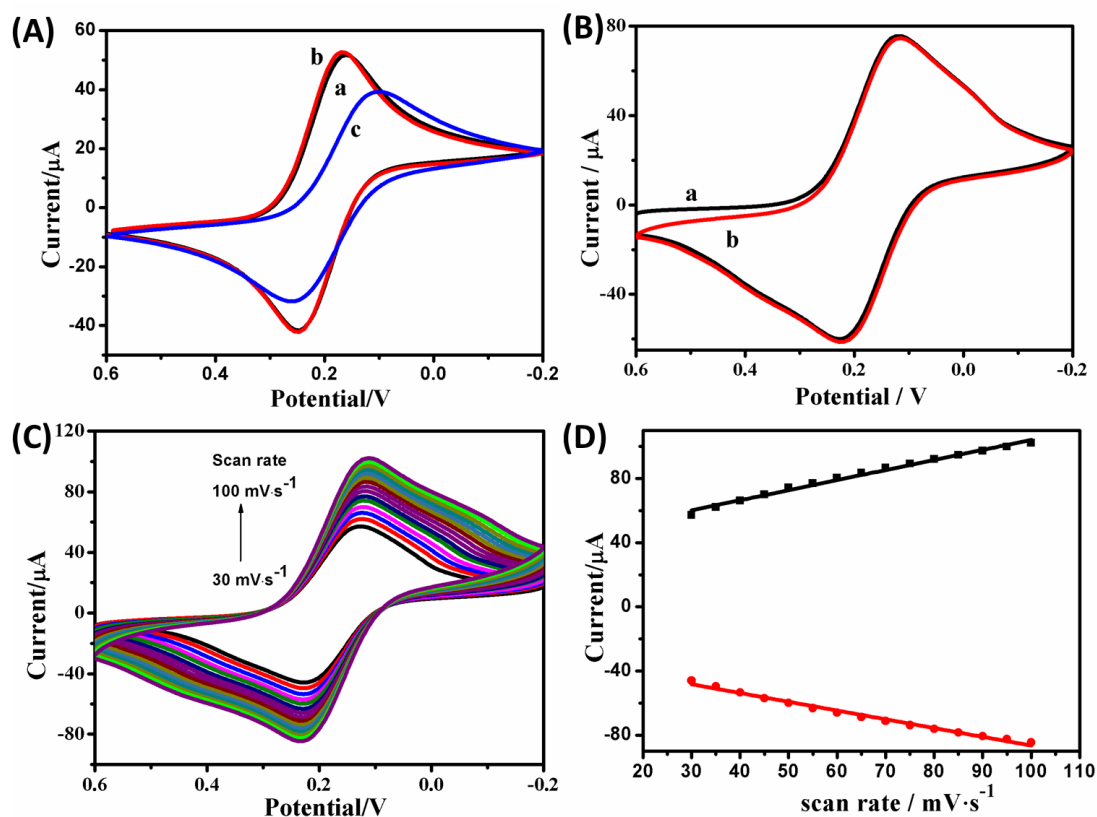


**Figure 4.** (A) CVs of (a) bare GCE (b) FF fibrils/GCE and (c) FF powder/GCE. (B) FF fibrils modified electrode at cyclic numbers of (a)1<sup>st</sup> and (b) 100<sup>th</sup>. (C) CVs of FF fibrils/GCE at different scan rates: 30, 35, 40, 45, 50, 55, 60, 65, 70, 75, 80, 85, 90, 95 and 100  $\text{mV}/\text{s}$ , respectively (D) Plots of cathodic and anodic peak currents against scan rate.

These results show that FF fibrils film, which was facilely self-assembled on the electrode, has good adsorbability. The effect of scan rate on the current response of FF fibrils was also investigated (Fig. 4C). The peak currents of cathode and anode increased, and the peak potentials exhibit a small shift as the scanning rate increased from 30 to 100  $\text{mV}\cdot\text{s}^{-1}$ . The cathodic and anodic peak currents were in linear proportion to the scan rate with the correlation coefficients (R) values of 0.9953 and 0.9949, respectively (Fig. 4D). The results demonstrate that the reaction is a quasi-reversible and surface controlled electrochemical process.

### 3.2 Hydrogen peroxide biosensor based on FF fibrils

HRP is widely used as a model enzyme for construction of electrochemical biosensors. The electrocatalytic reduction of  $\text{H}_2\text{O}_2$  on the HRP/GCE and HRP/FF fibrils/GCE is studied (Fig. 5). Only non-faradic signals were observed with HRP/GCE after adding  $1.0\times 10^{-5}$  M  $\text{H}_2\text{O}_2$  (Fig. 5A). In contrast, an obvious improvement in the cathodic current at the HRP/FF fibrils/GCE was obtained in the presence of  $1.0\times 10^{-5}$  M  $\text{H}_2\text{O}_2$ , which indicates that triggers a bioelectrocatalytic reaction. The current response of the biosensor increased along with  $\text{H}_2\text{O}_2$  concentration.

The pH value of the buffer solution has influence on the sensitivity of biosensors. The experimental results in the current study at pH 5.5-8.0 showed that the current increases with pH up until pH 7.0, and then decreased. The high response current at neutral pH may be due to high enzyme activity. Optimization of applied potential on working electrode is the basis for reaching a low detection limit and avoiding electrochemical interference. The effects of working potentials were investigated and an optimized potential of -0.7 V was selected.

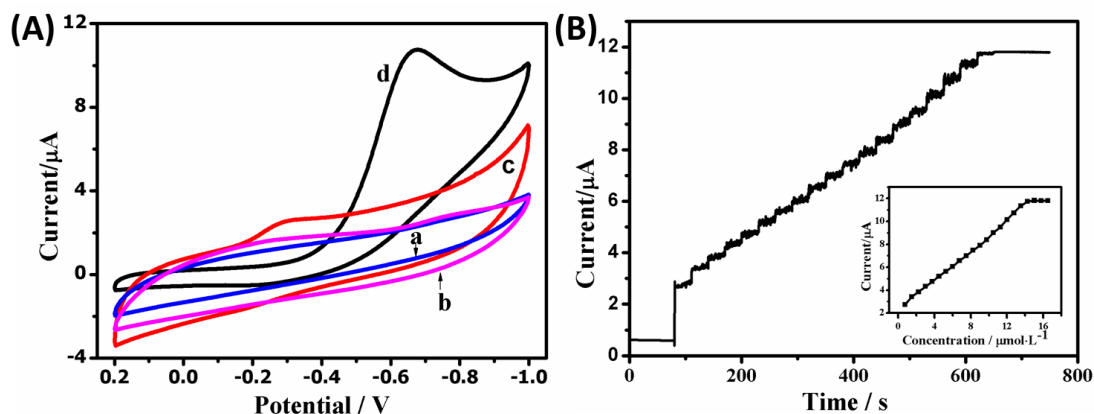


**Figure 5.** (A) Cyclic voltammograms of (a) HRP/GCE, (c) HRP/FF fibrils/GCE in 0.1 M PBS (pH=7.0) and (b)HRP/GCE, (d) HRP/FF fibrils/GCE adding  $1.0 \times 10^{-5}$  M  $H_2O_2$ . Scan rate: 100 mV/s (B) Amperometric response of the HRP/FF fibrils/GCE at -0.7 V upon successive additions of  $H_2O_2$  to PBS (pH 7.0). Inset: the current responses vs.  $H_2O_2$  concentration.

Amperometric measurements are in wide use to evaluate the performance of electrochemical enzyme sensors. Fig.5B shows typical amperometric responses of the HRP/FF fibrils/GCE with successive additions of  $0.75 \mu\text{M}$   $H_2O_2$  to PBS (pH 7.0) at a potential of -0.7 V. The reduction currents rise step by step at the HRP/FF fibrils/GCE. When the concentration of  $H_2O_2$  was higher than  $1.4 \times 10^{-5}$  M, a plateau was observed (inset in Fig.5B). This curve showed a characteristic of the Michaelis–Menten relationship. The apparent Michaelis-Menten constant ( $K_M^{app}$ ) is an indicator of enzyme-substrate kinetics. The  $K_M^{app}$  can be calculated using the Lineweaver-Burk equation:

$$\frac{1}{I_{cat}} = \frac{1}{I_{max}} + \frac{K_M^{app}}{I_{max} C_{H_2O_2}}$$

Where  $I_{cat}$  is the electrocatalytic current,  $I_{max}$  is the maximum current measured under saturated substrate conditions, and  $C_{H_2O_2}$  is the bulk concentration of  $H_2O_2$ .  $K_M^{app}$  can be obtained by the analysis of slope and intercept of the plot of the reciprocals of the steady-state current versus  $H_2O_2$  concentration. The  $K_M^{app}$  value was calculated to be  $29.1 \mu\text{M}$ , indicating the higher catalytic activity of the HRP/FF fibrils film toward the reduction of  $H_2O_2$ . A lower value means that the substrate has a strong affinity for the enzyme, which facilitates its catalytic reaction. The corresponding calibration curve of the FF-based  $H_2O_2$  enzyme sensor exhibits a linear response in the concentration range from  $7.5 \times 10^{-7}$  to  $1.4 \times 10^{-5}$  M ( $R^2=0.997$ ), with a detection limit of  $2.6 \times 10^{-7}$  M ( $S/N=3$ ) and a sensitivity of  $0.65 \mu\text{A} \cdot \text{cm}^{-2} \cdot \mu\text{M}^{-1}$ . The comparison of the developed method with the previous methods was made to

evaluate the analytical performance (Table 1). The obtained results are comparable with the other reported in the literature [37-40]. The good performances were mainly attributed to the FF fibrils, which provided a large surface area. The biosensor response reaches 95% of a steady-state value within about 1.5 s at each H<sub>2</sub>O<sub>2</sub> injection, indicating a fast electron transfer process. We also investigated the storage ability of the HRP/FF fibrils/GC electrode by comparing the changes in the current response. The electrode was stored at 4°C for 7 days, and the response of sensor only decreased 6.9%. To study the reproducibility of the HRP/FF fibrils, we also repeated a series of successive measurements, and the results show an acceptable reproducibility in the current response to the 5×10<sup>-6</sup> M H<sub>2</sub>O<sub>2</sub> with a RSD of 4.7%. These results demonstrate that the HRP/FF fibrils/GCE has a good storage stability and reproducibility, which could be attributed to the good film forming ability and excellent biocompatibility of organic FF fibrils.

**Table 1.** Comparison of the proposed method with the previous works.

Electrode	LOD (μM)	Sensitivity (μA·μM <sup>-1</sup> ·cm <sup>-2</sup> )	Linear range (μM)	Reference
HRP/FF fibrils	0.26	0.65	0.75-14	This work
HRP/Graphene-Fe <sub>3</sub> O <sub>4</sub>	0.6	0.132	5-3810	37
CeO <sub>2</sub> NP/N-rGO	1.3	0.036	1.8-920.8	38
copper nanoparticles	3.4	--	8-70	39
Fe <sub>3</sub> O <sub>4</sub> /GO-PAMAM	2.0	--	20-1000	40

To test the practicability, the HRP/FF fibrils modified electrode was used to determine H<sub>2</sub>O<sub>2</sub> in the local tap water and commercial mineral water and the results were illustrated in Table 2. The recoveries were in the range of 98.0-103.1% with the RSD in the range of 2.7-4.3%. These results confirm that the FF fibrils electrochemical biosensor was suitable for the determination of hydrogen peroxide in simple water samples with satisfactory accuracy.

**Table 2.** Detection of hydrogen peroxide in water samples by the proposed method (n=3)

Samples	Results	Added (μM)	Found (μM)	Recovery (%)	RSD (%)
Mineral water	Not found	1.00	0.98	98.0	2.7
		10.00	10.31	103.1	4.3
Tap water	Not found	1.00	0.94	94.0	3.8
		10.00	9.79	97.9	3.6

#### 4. CONCLUSIONS

In conclusion, FF peptide fibrils were prepared using cationic surfactant assisted evaporation induced self-assembly under mild conditions. Long persistence length peptide fibrils with ultra-high aspect ratio over 1000 were obtained. We demonstrate that modifying with the peptide fibrils can significantly enhance the sensitivity and ability of the electrochemical biosensor. This was assigned to the good film forming ability, excellent biocompatibility and higher aspect ratio. This facile bottom-up

method will open a new route for the growth of ultra-long 1D peptide materials, and may offer a novel platform for biosensors design and fabrications.

#### ACKNOWLEDGEMENT

This work was supported by the National Key Research and Development Program of China (2016YFD0401204), the National Natural Science Foundation of China (31501397), the Fundamental Research Funds for the Central Universities (JUSRP51714B) and National first-class discipline program of Food Science and Technology (JUFSTR20180303).

#### References

1. E. Shima, A. Nawal, R. A. M. Abdel, D. Majed; S. K. M. Ab, Z. Mohammed, *Biosens. Bioelectron.*, 101 (2018) 282.
2. X.X. Ge, A.M. Asiri, D. Du, W. Wen, S.F. Wang, Y.H. Lin, *Anal. Chem.*, 58 (2014) 31.
3. N.J. Ronkainen, H.B. Halsall, W.R. Heineman, *Chem. Soc. Rev.*, 39 (2010) 1747.
4. S. Fleming, R.V. Ulijn, *Chem. Soc. Rev.*, 43 (2014) 8150.
5. I.W. Hamley, *Peptide Nanotubes. Angew. Chem. Int. Edit.*, 53 (2014) 6866.
6. C.Q. Yuan, S.K. Li, Q.L. Zou, Y. Ren, X.H. Yan, *Phys. Chem. Chem. Phys.*, 19 (2017) 23614.
7. R.V. Ulijn, A.M. Smith, *Chem. Soc. Rev.*, 37 (2008) 664.
8. M. Reches, E. Gazit, *Science*, 300 (2003) 625.
9. K.B. Andersen, J. Castillo-Leon, M. Hedstrom, W.E. Svendsen, *Nanoscale*, 3 (2011) 994.
10. L. Adler-Abramovich, N. Kol, I. Yanai, D. Barlam, R.Z. Shneck, E. Gazit, I. Rouso, *Angew. Chem. Int. Edit.*, 49 (2010) 9939.
11. J. Ryu, C.B. Park, *Biotechnol. Bioeng.*, 105 (2010) 221.
12. C. Guo, Y. Luo, R.H. Zhou, G.H. Wei, *ACS Nano*, 6 (2012) 3907.
13. J. Jeon, C.E. Mills, M.S. Shell, *J. Phys. Chem. B*, 117 (2013) 3935.
14. X. Gao, F. Lu, B. Dong, Y. Liu, Y. Gao, L. Zheng, *Chem. Commun.*, 51 (2015) 843.
15. J. Xiao, L. Qi, *Nanoscale*, 3 (2011) 1383.
16. C.H. Gorbitz, *Chem. Commun.*, 22 (2006) 2332.
17. C.W. Hsu, G.J. Wang, *Biosens. Bioelectron.*, 56(2014) 204.
18. Y.X. Tang, Y.Y. Zhang, J.Y. Deng, D.P. Qi, W.R. Leow, J.Q. Wei, S.Y. Yin, Z.L. Dong, R. Yazami, Z. Chen, X.D. Chen, *Angew. Chem. Int. Edit.*, 53 (2014) 13488.
19. J.M.M. Moreno, M. Waleczek, S. Martens, R. Zierold, D. Gorbitz, V.V. Martinez, V.M. Prida, K. Nielsch, *Adv. Funct. Mater.*, 24 (2014) 1857.
20. L.Y. Li, Y. Liu, X.Y. Zhao, Z.Y. Lin, C.P. Wong, *ACS Appl. Mater. Inter.*, 6 (2014) 575.
21. H. Yoo, J. Sharma, H.C. Yeh, J.S. Martinez, *Chem. Commun.*, 46 (2010) 6813.
22. A. Aggeli, M. Bell, N. Boden, J. Keen, P. Knowles, T. McLeish, M. Pitkeathly, S. Radford, *Nature*, 386 (1997) 259.
23. A. Barth, C. Zscherp, *Q. Rev. Biophys.*, 35 (2002) 369.
24. K. Elfrink, J. Ollesch, J. Stöhr, D. Willbold, D. Riesner, K. Gerwert, *Proc. Natl. Acad. Sci. USA*, 105 (2008) 10815.
25. M.S. Lamm, K. Rajagopal, J.P. Schneider, D.J. Pochan, *J. Am. Chem. Soc.*, 127 (2005) 16692.
26. W.K. Surewicz, H.H. Mantsch, D. Chapman, *Biochemistry*, 32 (1993) 389.
27. D.R. Scheuing, J.G. Weers, *Langmuir*, 6 (1990) 665.
28. H.A. Behanna, J.J. Donners, A.C. Gordon, S.I. Stupp, *J. Am. Chem. Soc.*, 127 (2005) 1193.
29. M. Du, P. Zhu, X. Yan, Y. Su, W. Song, J. Li, *Chem. Eur. J.*, 17 (2011) 4238
30. M.O. Guler, S. Soukasene, J.F. Hulvat, S.I. Stupp, *Nano Lett.*, 5 (2005) 249.
31. M. Zhou, A.M. Smith, A.K. Das, N.W. Hodson, R.F. Collins, R.V. Ulijn, J.E. Gough, *Biomaterials*, 30 (2009), 2523.

32. A. Ajayaghosh, C. Vijayakumar, R. Varghese, S.J. George, *Angew. Chem. Int. Edit.*, 118 (2006) 470.
33. S. Gadde, E.K. Batchelor, J.P. Weiss, Y. Ling, A.E. Kaifer, *J. Am. Chem. Soc.*, 130 (2008) 17114.
34. G. Lu, Y. Chen, Y. Zhang, M. Bao, Y. Bian, X. Li, J. Jiang, *J. Am. Chem. Soc.*, 130 (2008) 11623.
35. A.M. Smith, R.J. Williams, C. Tang, P. Coppo, R.F. Collins, M.L. Turner, A. Saiani, R.V. Ulijn, *Adv. Mater.*, 20 (2008) 37.
36. L. Adler-Abramovich, M. Badihi-Mossberg, E. Gazit, J. Rishpon, *Small*, 6 (2010) 825.
37. K. Zhou, Y. Zhu, X. Yang, C. Li, *Electroanalysis*, 23 (2011) 862.
38. S. Yang, G. Li, G. Wang, L. Liu, D. Wang, L. Qu, *J. Alloys Compd.*, 688 (2016) 910.
39. J. Sophia, G. Muralidharan, *Mater. Res. Bull.* 70 (2015) 315.
40. X. Yang, L.N. Wang, G.Z. Zhou, N. Sui, Y.X. Gu, J. Wan, *J. Clust. Sci.*, 26 (2015) 789.

© 2018 The Authors. Published by ESG ([www.electrochemsci.org](http://www.electrochemsci.org)). This article is an open access article distributed under the terms and conditions of the Creative Commons Attribution license (<http://creativecommons.org/licenses/by/4.0/>).